ACS APPLIED MATERIALS & INTERFACES

Research Article

www.acsami.org

# Alginate/Nanohydroxyapatite Scaffolds with Designed Core/Shell Structures Fabricated by 3D Plotting and in Situ Mineralization for Bone Tissue Engineering

Yongxiang Luo,*[,†,‡] Anja Lode,[‡] Chengtie Wu,[†] Jiang Chang,[†] and Michael Gelinsky*[,‡]

[†]State Key Laboratory of High Performance Ceramics and Superfine Microstructure, Shanghai Institute of Ceramics, Chinese Academy of Sciences, Shanghai 200050, PR China

[‡]Center for Translational Bone, Joint and Soft Tissue Research, Medical Faculty and University Hospital, Technische Universität Dresden, 01069 Dresden, Germany

Supporting Information

**ABSTRACT:** Composite scaffolds, especially polymer/hydroxyapatite (HAP) composite scaffolds with predesigned structures, are promising materials for bone tissue engineering. Various methods including direct mixing of HAP powder with polymers or incubating polymer scaffolds in simulated body fluid for preparing polymer/HAP composite scaffolds are either uncontrolled or require long times of incubation. In this work, alginate/nano-HAP composite scaffolds with designed pore parameters and core/shell structures were fabricated using 3D plotting technique and in situ mineralization under mild conditions (at room temperature and without the use of any organic solvents). Light microscopy, scanning electron microscopy, microcomputer tomography, X-ray diffraction, and Fourier transform infrared spectroscopy were applied to characterize the fabricated scaffolds. Mechanical properties and protein delivery of the scaffolds were evaluated, as well as the cell response to the scaffolds by culturing human bone-marrow-derived mesenchymal stem cells (hBMSC). The obtained data indicate that this method is suitable to fabricate alginate/nano-HAP composite scaffolds with a layer of nano-HAP, coating the surface of the alginate strands homogeneously and completely. The surface mineralization enhanced the mechanical properties and improved the cell attachment and spreading, as well as supported sustaining protein release, compared to pure alginate scaffolds without nano-HAP shell layer. The results demonstrated that the method provides an interesting option for bone tissue engineering application.

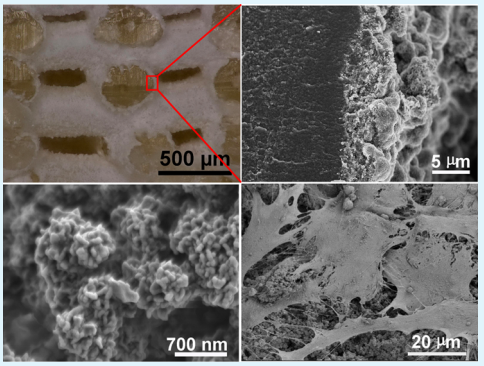


**KEYWORDS:** *alginate, composite scaffold, 3D plotting, in situ mineralization, bone tissue engineering*

## 1. INTRODUCTION

For repairing bone defects, for example, those caused by trauma, and for regenerating bone function, autologous bone is still being considered as "gold standard" in clinic.[1] However, the drawbacks of autografting including limited availability and donor site morbidity have forced scientists to search for alternatives via tissue engineering. Tissue engineering strategies require living cells, growth factors, synthetic porous scaffold and a bioreactor system.[2] The scaffold plays an important role in this process by providing sufficient mechanical support and mimicking the natural extracellular matrix (ECM).[3,4]

The materials for preparing scaffolds for tissue engineering should meet requirements such as biocompatibility and biodegradibility. Alginate is a biocompatible and degradable natural polymer, consisting of the two monosaccharide units: guluronic acid and mannuronic acid, which has been widely used for drug and growth factor delivery, cell encapsulation, and as scaffold in tissue engineering.[5−10] It forms a stable hydrogel when mixed with di- or trivalent cations like $Ca^{2+}$. These cations interact ionically with negatively charged carboxy groups of the guluronic acid units of the polysaccharide chain, which are stacked to form an egg-box-like structure, thus resulting in the formation of 3D gel networks. Gelation is based only on noncovalent interactions and therefore is fully reversible.[11,12] Although there are drawbacks such as lack of bioactivity and low compressive strength and modulus, alginate scaffolds still hold the potentials for being used in bone tissue engineering because of the capability of delivery growth factors and even living cells. Modification by introducing inorganic materials (especially hydroxyapatite (HAP)) is an option to improve the mechanical properties and bioactivity of alginate-based scaffolds. Some studies prepared alginate/HAP composite scaffolds with enhanced mechanical properties by direct mixing of alginate with HAP powder.[13,14] However, direct mixing is an uncontrolled method and results in a lack of homogeneity of particle distribution in the polymer matrix with limited bioactivity. Soaking scaffolds in simulated body fluid (SBF) or modified simulated body fluid (mSBF) is another

Received: December 2, 2014
Accepted: March 11, 2015
Published: March 11, 2015





DOI: 10.1021/am508469h
ACS Appl. Mater. Interfaces 2015, 7, 6541−6549

widely used method to prepare biopolymer/apatite composite scaffolds.[15−18] For example, Suárez-González et al. fabricated alginate/hydroxyapatite composite scaffolds by incubating alginate scaffolds in mSBF. Over 28 days of incubation, a layer of HAP was deposited on the surface of alginate scaffolds, and cell attachment was improved on the mineral-coated alginate surface.[19] However, this method normally requires a long time of incubation, which results in a decrease of stability because of the exchange of the cross-linking ions ($Ca^{2+}$) and partial degradation. Furthermore, a long time of incubation also alters the release characteristics of any encapsulated therapeutic agents or biological factors during storage in SBF over such a long time.

In situ mineralization is another simple and effective method for preparing polymer/apatite composites.[20−24] This method was also used for fabricating polymer/apatite microspheres for drug or growth factor delivery, such as alginate/apatite microspheres.[25−28] Alginate solution was prepared by dissolving alginate powder in a solution containing phosphate ions, and then this solution was dropped into a calcium chloride solution. The alginate was cross-linked with calcium ions and formed stable microspheres, and simultaneously, calcium ions reacted with phosphate ions to form hydroxyapatite. Although the alginate/apatite microspheres showed a sustained delivery of drugs, they had no apparent core/shell structure and according to our knowledge, there were no reports so far on fabricating alginate/apatite 3D scaffolds with predesigned structures and distinct core/shell morphology. Fibrous alginate/hydroxyapatite nanocomposite scaffolds can also be achieved via in situ mineralization by electrospinning,[29] but those more membranelike constructs lack predesigned macropores for cell penetration and ingrowth of new tissue.

Therefore, in this study, we describe the fabrication of novel alginate/apatite core/shell scaffolds with predesigned structure by 3D plotting and in situ mineralization based on highly concentrated alginate pastes under mild conditions (at room temperature and without the use of any organic solvents). The 3D plotting technique is able to fabricate scaffolds with predefined outer and inner structure and shape[30−34] compared to other conventional methods such as particle leaching and freeze-drying. The scaffolds were characterized by light microscopy, scanning electron microscopy (SEM), microcomputer tomography ($\mu$-CT), X-ray diffraction (XRD), and Fourier transform infrared spectroscopy (FTIR). Furthermore, the mechanical properties, cytocompatibility, and protein delivery ability were investigated.

## 2. MATERIALS AND METHODS

**2.1. Fabrication of Scaffolds.** For fabricating the mineralized alginate scaffolds, the alginate pastes were first prepared by mixing sodium alginate powder (Manugel; ISP Alginates Ltd. Waterfield, Tadworth, U.K.) with freshly prepared aqueous 500 mM $Na_2HPO_4$ (Sigma-Aldrich, Taufkirchen, Germany) solution in a mass ratio of 1:5.5. The pastes were stirred until they became homogeneous and then filled into a plotting cartridge. 3D scaffolds were fabricated by extruding the pastes through nozzles (inner diameter was 0.6 mm) layer by layer by a 3D plotting system which was developed by Fraunhofer IWS (Dresden) on the basis of the Nano-Plotter from GeSiM (Grosserkmannsdorf, Germany). The moving speed of the plotting head was 4 mm/s, and the dosing pressure was 4.5−5.5 bar. After scaffolds were plotted in air, they were transferred to a 1 M $CaCl_2$ solution, in which the pH value was adjusted to 9.5 by Tris buffer. An as-received $CaCl_2$ solution (pH 5) without adjustment of pH value was used as control. After incubation in the $CaCl_2$ solution for 30 min, the scaffolds were washed with deionized water and then dried at room temperature. As control, pure alginate and mixed alginate/HAP scaffolds were fabricated with the same process by either mixing only alginate or alginate with HAP powder (Merck, Darmstadt, Germany) in a mass ratio of 3:1 with deionized water instead of $Na_2HPO_4$ solution. The average size ($d_{50}$) of the HAP particles was 2.3 $\mu$m, and the size distribution (range of $d_{10}$−$d_{90}$) was 0.9−4.8 $\mu$m.

**2.2. Characterization of Scaffolds.** The pore size and shape as well as surface morphologies of scaffolds were characterized by light microscopy (stemic 2000-C, Zeiss, Germany). The samples were cut with a razor blade, coated with carbon, and analyzed by SEM (DSM 982-Gemini, Zeiss, Oberkochen, Germany) and energy dispersive spectrometry (EDS). $\mu$-CT was applied to demonstrate the 3D structures of the scaffolds. The tomographic examinations were carried out with a $\mu$-CT imaging apparatus, which was based on a nanofocus tube with the transmission target of the product line phoenix/X-ray (GE Measurement and Control Solutions, USA). The focal spot diameter of the tube was 0.65 $\mu$m for the used mode 1. The detection of X-rays has been performed with a Shad-o-Box 4K (Rad-icon Imaging Corp., USA), which comprises a $Gd_2O_2S$ scintillator and a photodiode array. XRD (Bruker D8 with area detector Vantec 2000, Bruker, Germany) and FTIR (Spectrum 2000, PerkinElmer, USA) were also used to analyze the composites and phases of mineralized scaffolds. The shrinkage of scaffolds was calculated by dividing the change of the size before and after drying with the size before drying. Water adsorption was performed by incubating scaffolds in deionized water at 37 °C. At 1 and 3.5 h, three scaffolds for each type were taken out from water and put on a filter paper for a few seconds to remove the water from the macropores and then weighed. The water adsorption was calculated by dividing the weight change with the dry weight of the scaffolds before incubation in water.

**2.3. Mechanical Test.** Compressive tests were carried out on dry and wet scaffolds (without and with soaking in SBF for 2 h at 37 °C) by a mechanical testing machine (INSTRON 5566, Germany) with a load cell of 10 kN and a cross-head speed of 1.0 mm/min. Scaffolds with size of 10 × 10 × 10 mm were plotted for compressive test. Compression of 25% strain in $z$ direction was performed for all samples without breakage. The received data were used to calculate the compressive modulus (of elasticity). The modulus was taken from the slope of the stress−strain curves in the elastic deformation region. Five samples were tested for mean and standard deviation calculation.

**2.4. Cell Culture Experiment with hBMSC.** Seeding and cultivation of human bone-marrow-derived mesenchymal stem cells (hBMSC) was performed according to our previous publication.[33,34] Human BMSC were provided by the Medical Clinic I, Dresden University Hospital Carl Gustav Carus (Prof. Bornhäuser and coworkers). The ethics commission of the Technische Universität Dresden approved the application of hBMSC for in vitro experiments (EK263122004). The cells were cultivated in Dulbecco's modified Eagle's medium low-glucose (DMEM) (Biochrom, Berlin, Germany) containing 9% fetal calf serum (Biochrom), 100 U/ml penicillin, and 100 $\mu$g/mL streptomycin (Biochrom) at 37 °C and 8% $CO_2$.

Prior to cell seeding, scaffolds with a size of 5 × 5 × 3.5 mm were preincubated in culture medium for 24 h. Afterward, the samples were placed on sterile filter paper to remove excess liquid from the pores and set into 48-well polystyrene culture plates. Each scaffold was seeded with 5.5 × $10^5$ cells (passage 5) within 400 $\mu$L of medium. At 24 h after seeding, the cell-seeded scaffolds were transferred to fresh culture dishes. Cultivation was carried out in the presence of osteogenic supplements ($10^{-7}$ M dexamethasone, 3.5 mM $\beta$-glycerophosphate, and 0.05 mM ascorbic acid 2-phosphate (all purchased from Sigma-Aldrich)).

The number of viable cells in the scaffolds was quantified by measurement of cytosolic lactate dehydrogenase (LDH) activity in the lysates using the CytoTox 96 Non-Radioactive Cytotoxicity Assay (Promega, Madison, USA) according to the manufacturer's instructions. Absorbance was measured at 492 nm with a multifunction microplate reader (SpectraFluor Plus, Tecan, Crailsheim, Germany) and correlated with the cell number using a calibration line.


DOI: 10.1021/am508469h
ACS Appl. Mater. Interfaces 2015, 7, 6541−6549

To evaluate osteogenic differentiation of hBMSC, specific alkaline phosphatase (ALP) activity was determined. Aliquots of the lysates were incubated with 1 mg/mL *p*-nitrophenylphosphate (Sigma-Aldrich) in 0.1 M diethanolamine (pH 9.8) containing 1% Triton X-100 and 1 mM $MgCl_2$ at 37 °C for 30 min. NaOH (1 M) was added to stop the enzymatic reaction, and the absorbance was read at 405 nm (SpectraFluor Plus, Tecan). A calibration line consisting of different dilutions of a 1 mM *p*-nitrophenol (*p*Np) stock solution was used to calculate the amount of *p*Np. To determine the specific ALP activity (in $\mu$mol *p*Np/30 min/$10^6$ cells), the *p*Np amount was related to the respective cell number (calculated from the LDH activity).

The morphology of the cells attached to the scaffolds was observed by SEM. Scaffolds seeded with cells were washed twice with PBS, then fixed with 3.7% formaldehyde in 100 mM $CaCl_2$ solution for 30 min, washed with distilled water, and dehydrated using a gradation series of ethanol/distilled water solutions. Critical-point drying was performed with a CPD 030 apparatus (BAL-TEC AG, Liechtenstein). Dry samples were coated with gold, and imaged using a Philips XL 30/ESEM with FEG (field emission gun).

**2.5. Bovine Serum Albumin Loading and Release Study.** Bovine serum albumin (BSA), used as a model protein, was selected to study the protein delivery ability from the plotted scaffolds. First, 100 mg BSA was dissolved in 10 mL of 500 mM $Na_2HPO_4$ solution or water. Then 1 g of alginate or alginate/HAP was mixed with 5.5 g of $Na_2HPO_4$ solution or water (in which BSA was already dissolved) to prepare the plotting pastes. Thereby, the BSA amount in 1 g of the prepared pastes is

$$100\ \text{mg}/10\ \text{mL} \times (5.5/6.5 \times 1\ \text{g})/\rho\ \text{g/mL}$$

The scaffolds were prepared according to the description in section 2.1. Before transferring the scaffolds to $CaCl_2$ solution for cross-linking, they were weighed in the wet state to calculate the loaded amount of BSA according to the formula

$$M_{BSA} = 10 \times (5.5/6.5 \times W_s)/\rho\ \text{mg}$$

where $M_{BSA}$ is the amount of loaded BSA in scaffold, $W_s$ is the weight of wet scaffold, and $\rho$ is the density of solution (500 mM $Na_2HPO_4$ or water). Afterward, each scaffold was immersed in 5 mL of 1 M $CaCl_2$ solution (pH 9.5) for 30 min and then washed three times with 15 mL of deionized water. The remaining $CaCl_2$ solution was collected and analyzed by UV absorption (UV min-1240, Shimadzu, Japan) at 280 nm. The data were used to calculate the BSA loading efficiency according to the formula represented as

$$P_{BSA} = 1 - (M_{loss}/M_{BSA})$$

where $P_{BSA}$ is BSA loading efficiency and $M_{loss}$ is the amount of BSA in the remaining $CaCl_2$ solution.

After drying, each of the BSA-loaded scaffolds was immersed in 6 mL SBF solution (pH 7.4) and kept at 37 °C. At each designed time point, 3 mL SBF were taken, filled in 15 mL test tubes and centrifuged at 4000 rpm for 10 min. The supernatants were taken to quantify the released BSA content by UV absorption at 280 nm, calculated according to a calibration line. Finally, 3 mL fresh SBF were added to each sample. Three samples were tested for each type of scaffolds.

**2.6. Statistical Analysis.** All data presented as means ± standard deviation (SD). One-way ANOVA was performed to analyze the variables, and $p < 0.05$ was considered statistically significant.

## 3. RESULTS

**3.1. Fabrication and Characterization of Scaffolds.** The mineralized pastes prepared by mixing alginate powder with an aqueous $Na_2HPO_4$ solution with an alginate content of 15.4 wt % were excellently injectable and stable after plotting into scaffolds. When the plotted scaffolds were transferred to a $CaCl_2$ solution with pH 9.5, milky white layers were formed as a shell on the surface of the scaffolds as well as in the solution immediately. However, when soaking pure alginate and mixed alginate/HAP scaffolds (prepared with deionized water instead of $Na_2HPO_4$ solution) in a $CaCl_2$ solution, no apparent visible changes occurred, and the solutions remained clear. When incubating the alginate scaffolds containing phosphate ions in a $CaCl_2$ solution, calcium was consumed both by alginate gelation and by calcium phosphate formation.

Microscopical images in Figure 1 of dry scaffolds showed that the appearance of pure alginate scaffolds was brown, mixed alginate/HAP scaffolds were white and the HAP particles, embedded in the alginate strands, clearly could be observed. However, mineralized scaffolds formed at pH 5 were covered by layers of brushite ($CaHPO_4{\cdot}2\ H_2O$) crystals whereas scaffolds mineralized at pH 9.5 were covered by a layer of nano-HAP.

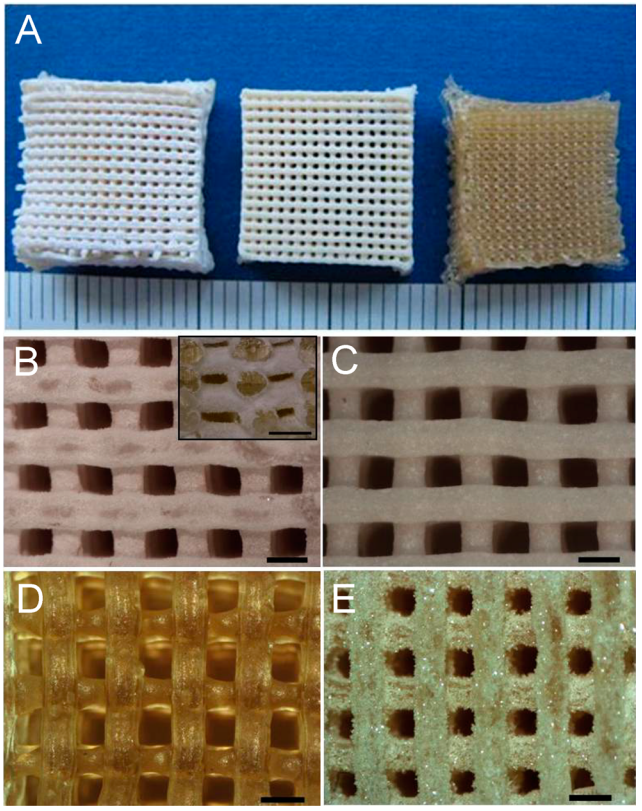


**Figure 1.** (A)Photograph of plotted scaffolds: from left to right, mineralized alginate (pH 9.5), mixed alginate/HAP and pure alginate. Microscopy images of (B) mineralized alginate (pH 9.5), (C) mixed alginate/HAP, (D) pure alginate, and (E) alginate mineralized at pH 5. Insert in B shows the core/shell morphology in a cross-sectional view. Scale bars: A, millimeters and B–E, 500 $\mu$m.

As shown in Figure 2, the SEM images revealed that the fabricated scaffolds had open and interconnected pores in all directions. High-magnification SEM showed that the mineralized alginate scaffolds prepared at pH 9.5 were completely covered by a layer of needlelike nanoapatite crystals on the surface. The formed core/shell structures with an alginate core and apatite shell of about 34 $\mu$m thickness were clearly observed. EDS analyses of the rough mineralized surface of these scaffolds showed strong calcium and phosphate signals. However, the surface of pure alginate scaffolds was smooth and dense, and EDS analysis showed only a calcium peak but not a phosphate peak. However, mixed alginate/HAP scaffolds were rougher, and the HAP in these, spread on and embedded inside the alginate strands, was distributed nonhomogeneously. In


DOI: 10.1021/am508469h
ACS Appl. Mater. Interfaces 2015, 7, 6541–6549

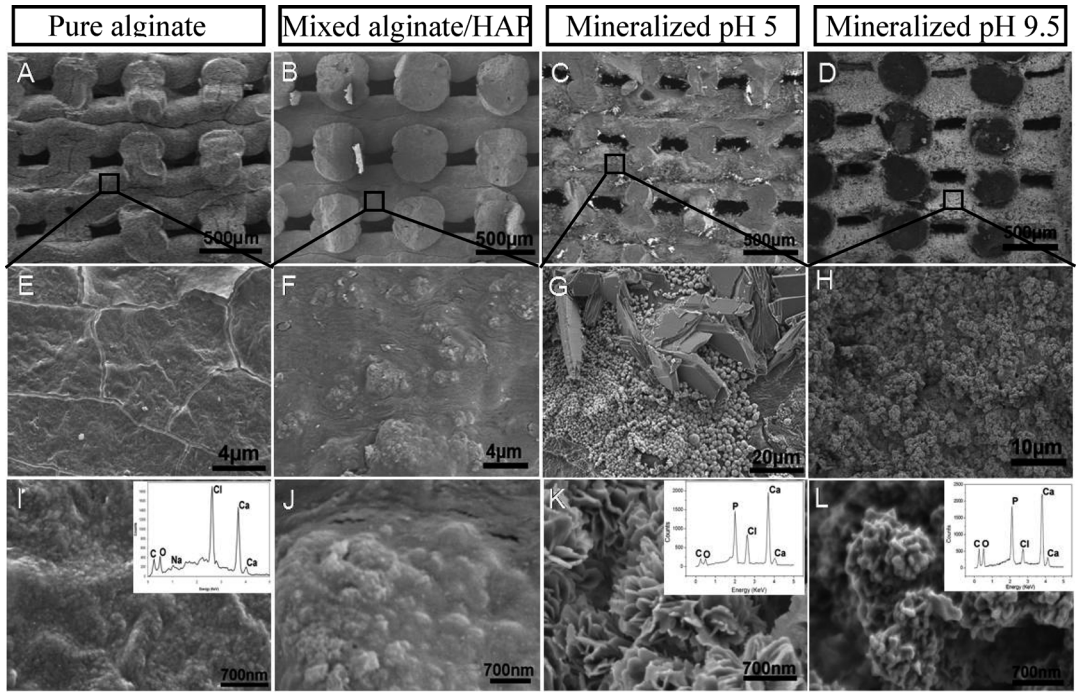


**Figure 2.** SEM images of (A, E, and I) pure alginate, (B, F, and J) mixed alginate/HAP, and alginate scaffold mineralized at (C, G, and K) pH 5 and (D, H and L) pH 9.5. (A–D) Cross-sectional view and (E–L) high magnification view of the surfaces. The inserts show corresponding EDS analyses.

contrast, microsized sheetlike brushite and nanosized roselike apatite crystals were deposited on the surface of mineralized alginate scaffolds at pH 5, but the scaffolds possessed no clear core/shell structure.

The $\mu$-CT data in Figure 3 also gave sufficient information about the novel core/shell scaffolds. From the obtained $\mu$-CT

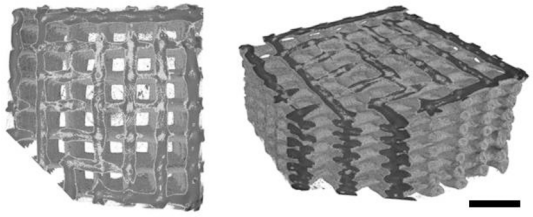

**Figure 3.** $\mu$-CT analysis of the mineralized alginate scaffold prepared at pH 9.5; (left) cross-sectional view and (right) over view. Scale bar = 1 mm.

images, it can be clearly seen that the pores of the scaffold were completely open and interconnected, even in the center of the constructs. A layer of X-ray-dense composite rich in calcium phosphate covers the entire surface of all strands throughout the whole scaffold.

XRD and FTIR (Figures 4 and 5, respectively) were applied to further characterize the scaffolds, and the data indicated that the characteristic XRD peaks for commercially available HAP were observed in the XRD pattern of the alginate scaffold mineralized at pH 9.5. As control, the XRD pattern of bare alginate without any apparent characteristic peaks is also presented. FTIR studies showed that the P–O bands (560 and 600 $cm^{-1}$) were clearly observed in the mineralized alginate scaffolds prepared at pH 9.5 compared to the pure alginate ones. Both of these indicated that the prepared mineral layer on the alginate scaffold was HAP.

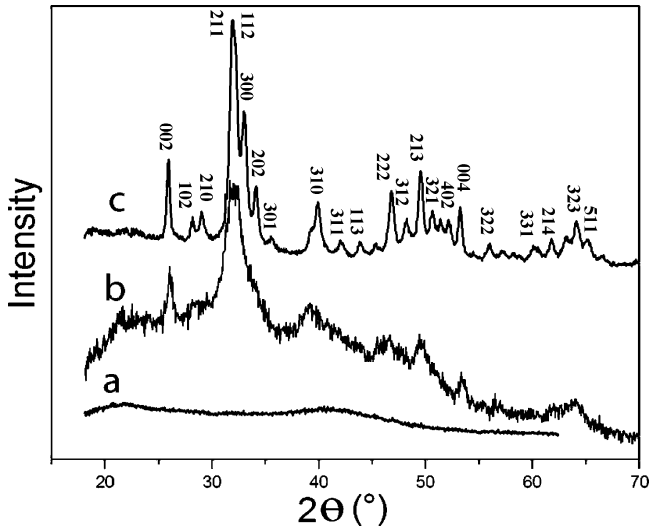


**Figure 4.** XRD patterns of pure alginate, mineralized alginate scaffold (pH 9.5), and pure HAP powder (labeled a–c, respectively).

Alginate scaffolds underwent certain shrinkage during drying. Here, we also characterized the shrinkage (Figure 6A) of the mineralized alginate scaffolds, and the results revealed that they suffered less shrinkage and deformation than pure alginate ones. The water adsorption (Figure 6B) of pure alginate and mineralized scaffolds in deionized water for 1 and 3.5 h seems to have no significant difference; however, both were higher than that of mixed alginate/HAP scaffolds.

**3.2. Mechanical Test of Scaffolds.** Compressive strength and modulus of the plotted scaffolds were tested in dry and wet conditions. The data (Figure 7) show that the compressive strength of plotted core/shell scaffolds is higher than that of pure alginate scaffolds (measured at 25% compressive strain),


DOI: 10.1021/am508469h
ACS Appl. Mater. Interfaces 2015, 7, 6541–6549

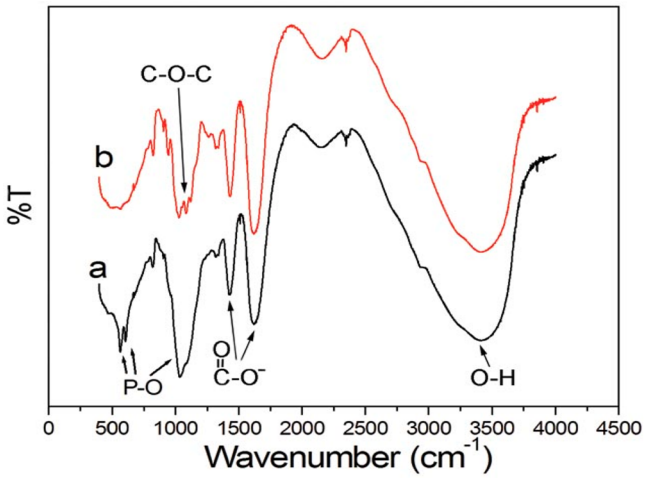


**Figure 5.** FTIR spectra of (a) mineralized alginate scaffold (pH 9.5) and (b) pure alginate scaffold.

in both dry and wet states. The compressive strength of core/shell alginate/apatite scaffolds was 30.7 ± 3.4 MPa at a compressive strain of 20% in dry state, and the strength increased linearly with the strain. Young's modulus of core/shell alginate/apatite scaffolds was 263.9 ± 94.1 MPa in the dry state and therefore also higher than that of pure alginate ones. However, the compressive strength and modulus decreased sharply in the wet state for pure alginate and mixed alginate/HAP scaffolds, as well as for core/shell alginate/apatite scaffolds.

**3.3. hBMSC Culture on the Scaffolds.** Figure 8 shows SEM pictures of hBMSC attached to pure alginate, mixed alginate/HAP, and mineralized alginate scaffolds on day 1 of culture. The cells attached and spread more favorably on the mineralized scaffolds, as indicated by a higher cell density and more pronounced filopodia on this scaffold type. This observation was especially in contrast to the poor cell attachment found on pure alginate scaffolds.

The number of viable cells on the scaffolds was determined by measurement of the LDH activity after 1 and 14 days of culture (Figure 9A). The data revealed that significantly more cells were attached 1 day after seeding on the mineralized alginate scaffolds than on pure alginate scaffolds. A slight increase of the cell number within 14 days of cultivation was observed for all three scaffold types. Still, a significantly higher cell number was detected on the mineralized scaffolds compared to the pure alginate scaffolds. Evaluation of ALP activity of the cells cultivated under osteogenic stimulation showed an increase over time with maximum values on day 14 for all three scaffold types (Figure 9B). Especially on day 14, but also on days 7 and 21, specific ALP activity determined for the mineralized alginate scaffolds was clearly higher compared to that of pure alginate and mixed alginate/HAP scaffolds.

**3.4. BSA Delivery.** Because of the mild preparation conditions (room temperature and no organic solvent used), growth factors can be loaded into the pasty materials and plotted to create scaffolds directly. In this study, we selected BSA as model protein to investigate the protein delivery ability from the plotted 3D scaffolds. Our data (Figure 10) indicated that the BSA has a high loading efficiency in mineralized core/shell scaffolds (92.6 ± 0.7%), which was significantly higher than that in pure alginate (67.5 ± 0.5%) and mixed alginate/HAP (78.2 ± 1.3%) scaffolds. BSA showed a sustained release from the plotted scaffolds, especially from the mineralized core/shell scaffolds, where BSA was released over 25 days.

## 4. DISCUSSION

In the present study, we fabricated mineralized alginate scaffolds with predesigned structure by 3D plotting and in situ mineralization. Our results demonstrate that this method is effective for fabricating alginate/apatite composite scaffolds with controlled core/shell structures. The mineralized scaffolds have enhanced mechanical properties compared to pure alginate scaffolds. In addition, the layer of nanoapatite formed in situ showed positive effects on hBMSC attachment compared to that of pure alginate. Finally, mineralized scaffolds had a sustained protein delivery capability, which is favorable for tissue engineering and drug delivery applications.

The concentrated alginate pastes (about 15 wt %) prepared with deionized water or $Na_2HPO_4$ solution were suitable for extrusion through fine plotting needles (inner diameter from 150 $\mu$m to 1 mm). Compared to those with a low concentration of alginate (≤4 wt %),[35] highly concentrated alginate pastes were able to form stable 3D scaffolds without deformation by directly plotting in air and did not require plotting in $CaCl_2$ solution for immediate cross-linking.[33,34]

After incubation of the alginate scaffolds prepared with phosphate ions in $CaCl_2$ solution, calcium was consumed both by mineral formation and by alginate gelation. Because of the low pH (pH 5) of the pure $CaCl_2$ solution, the main mineral formed was brushite.[34] However, when the pH value of the calcium chloride solution was adjusted to around 9.5, no

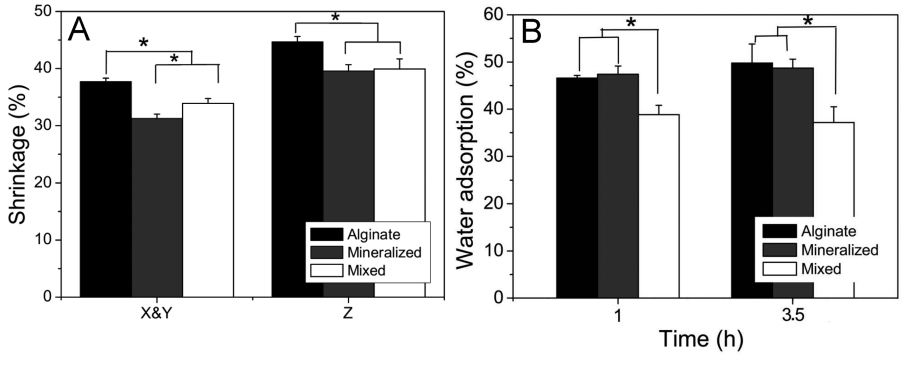


**Figure 6.** Shrinkage of scaffolds (A) in *x*, *y*, and *z* directions after drying at room temperature and (B) water adsorption of dried scaffolds after immersion in deionized water at 37 °C for 1 and 3.5 h. Mineralized alginate scaffolds were prepared at pH 9.5. (* = $p < 0.05$).



DOI: 10.1021/am508469h
ACS Appl. Mater. Interfaces 2015, 7, 6541−6549

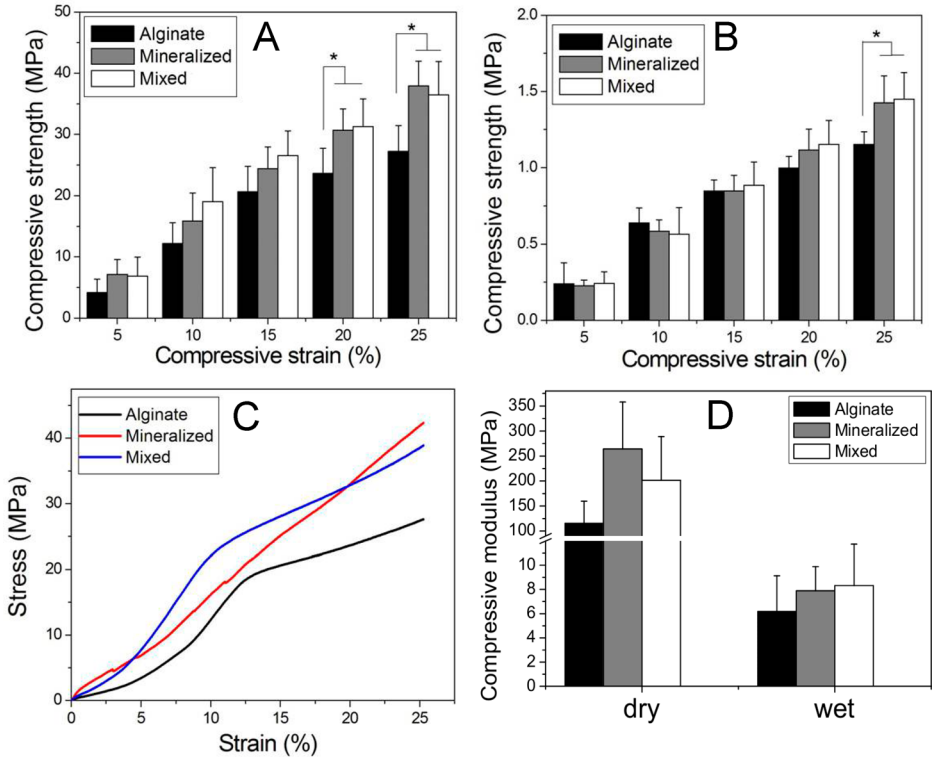


**Figure 7.** Compressive strength of scaffolds in (A) dry and (B) wet (immersion in SBF for 2 h at 37 °C) states and (C) typical strain−stress curves in dry state. (D) Young's modulus of scaffolds ($n$ = 5). Mineralized alginate scaffolds were prepared at pH 9.5 (* = $p < 0.05$).

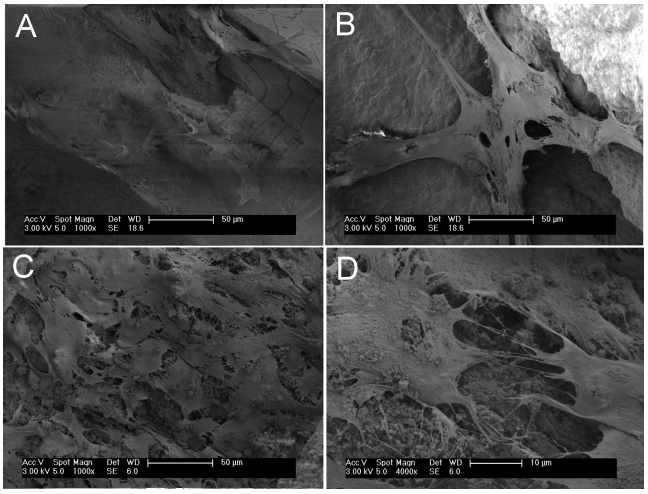


**Figure 8.** SEM images of hBMSC attached on (A) pure alginate scaffolds, (B) mixed alginate/HAP scaffold, and (C and D) mineralized alginate scaffold (pH 9.5) after 24 h of culture.

brushite was observed in the scaffolds, but only HAP formed.[36,37]

Interestingly, it seems that most of the minerals only developed on the surface of the alginate scaffolds, but few mineral phases appeared inside of the alginate strands. When the plotted scaffolds came in contact with $Ca^{2+}$-containing solution, a fast reaction of $Ca^{2+}$ and $PO_4^{3-}$ immediately took place at the surface of the alginate strands (as the interface between $Ca^{2+}$- and $PO_4^{3-}$-rich areas), leading to HAP formation. Because of the fast consumption of $PO_4^{3-}$ at the surface, phosphate ions from inside the strands (higher concentration) diffused to the surface (lower concentration) continually. At the same time, $Ca^{2+}$ diffused from the surface into the strands, but because of the inhibition by the fast-formed HAP shell and the consumption of calcium ions in the alginate cross-linking reaction, the $Ca^{2+}$ concentration decreased from the surface to the center of the strands. Therefore, HAP was mainly formed at the surface.

The apatite shell of the mineralized scaffolds was uniform and formed a continuous layer that had a certain contribution to the compressive behavior. The mixed alginate/HAP scaffolds also increased the mechanical properties compared to the pure alginate ones because of the mixed HAP powder that increased the density of the alginate strands. The compressive strength and Young's modulus of all the plotted scaffolds were remarkably lower in the wet state compared to those in the dry state. These three types of scaffolds were all plotted with alginate as the bulk structures. During drying, all scaffolds suffered more than 30% of shrinkage, and the strong shrinkage resulted in a significant increase of stiffness. However, after incubation in water, a significant amount of water was absorbed by the alginate strands. The water absorption led to swelling of the alginate strands that caused softening. The mixed alginate/HAP scaffolds had lower water adsorption capability compared to pure alginate and mineralized alginate scaffolds because the HAP particles mixed into the alginate paste occupied some space within the matrix and therefore decreased the ability for water adsorption.[38] The plotted alginate and mineralized scaffolds presented here have significantly higher mechanical strength than those fabricated with low concentrated alginate by either 3D plotting or conventional methods.[24,39−41] Reasons for the higher strength are (1) the higher solid content and (2) the reduced swelling capability compared to that of scaffolds manufactured from low-concentration alginate hydrogels.[33,34,42]



DOI: 10.1021/am508469h
ACS Appl. Mater. Interfaces 2015, 7, 6541−6549

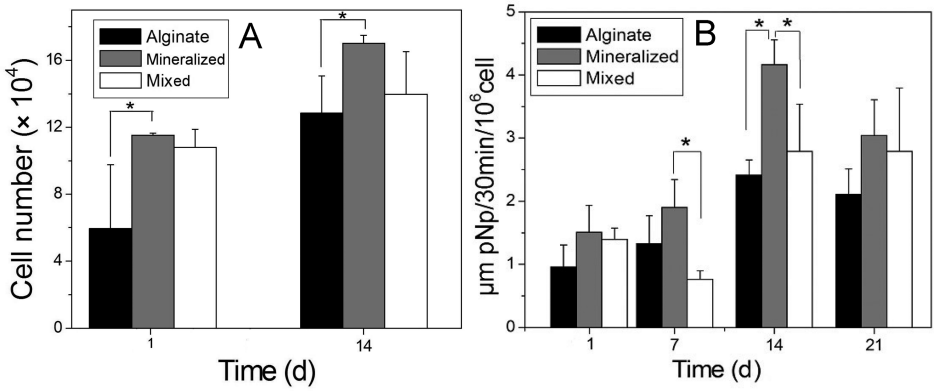


**Figure 9.** (A) Cell number and (B) specific ALP activity of hBMSC cultivated on the plotted scaffolds in culture medium with osteogenic supplements ($n$ = 4, mean ± SD, * = $p$ < 0.05).

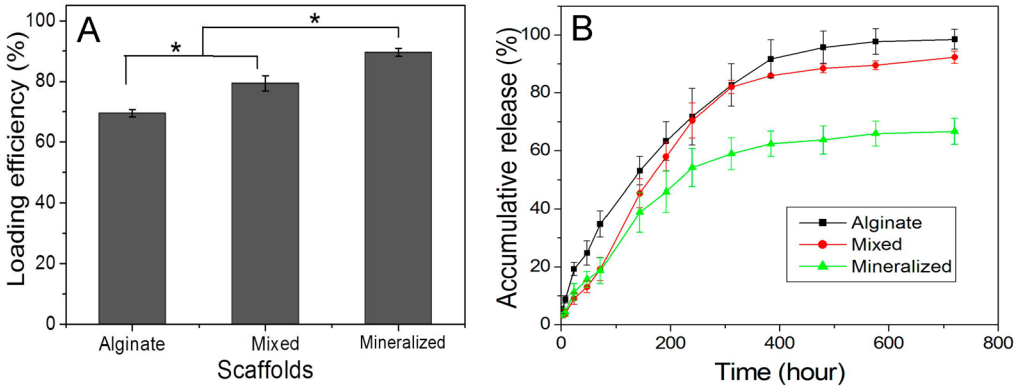


**Figure 10.** (A) BSA loading efficiency and (B) release behavior from scaffolds in SBF solution (pH 7.4, 37 °C, * = $p$ < 0.05).

There are many studies demonstrating the influence of surface properties of scaffolds on cell attachment and shape,[43−46] especially chemical composition and morphology. Surface characteristics strongly influence protein-binding ability, known to be one of the key factors for cell adhesion. The effect of extracellular matrix proteins on stem cell differentiation is well-reviewed.[47] It has been studied that alginate is not a perfect candidate for cell attachment because it lacks specific binding sites for cells and has a negative charge balance that inhibits adsorption of many proteins because of electrostatic repulsion.[48] However, this can be improved by modifying the surface properties of alginate, for example, via grafting with active peptides (like RGD).[49] The introduction of an apatite layer as demonstrated in this work changed the composition as well as the morphology of the scaffold surface, which therefore enhanced the cell attachment. Both the nanoapatite and the rougher surface might have contributed to the favorable attachment of hBMSC. Nanoapatite formation on the surface of scaffolds has been performed quite often by incubating scaffolds in SBF, and the formed apatite layer has been proven to have significant improvement for cell attachment.[19] The cell morphology observed on the mineralized scaffolds was much rounder and smaller compared to that on pure alginate scaffolds. The cell shape has a strong influence on function and fate of hBMSC.[50,51] It was shown that hBMSC have a smaller and more round shape on rougher surfaces and that cells with a smaller spread area tend to differentiate more.[52]

Our method for plotting alginate and core/shell scaffolds was performed under mild conditions (room or physiological temperature and without using any organic solvent) and in a highly efficient manner. It took less than 1 h from preparing plotting pastes to finish the cross-linking and in situ mineralization of the scaffold. Therefore, drugs and proteins (like growth factors) can be loaded into this system directly during scaffold preparation without denaturation. Through this method, the loading efficiency was very high, and the loaded amount of drugs and proteins can be controlled easily.

## 5. CONCLUSIONS

A novel alginate scaffold with a layer of nano-HAP coating was fabricated by a 3D plotting technique and in situ mineralization under mild conditions. The apparent core/shell structures were observed, and a uniform apatite layer covered all of the outer and inner surface of the scaffolds. The mineralized scaffolds enhanced the mechanical properties as well as cell attachment and differentiation compared to those of pure alginate scaffolds without an apatite shell. Because of the mild processing conditions, BSA was loaded into the scaffolds successfully during plotting with high loading efficiency and had a sustained release over 25 days.

## ■ ASSOCIATED CONTENT

### Supporting Information

Microscopic and SEM images of scaffolds, EDS, XRD, and TGA analysis of brushite and scaffolds, and confocal LSM of cells on scaffolds. This material is available free of charge via the Internet at http://pubs.acs.org.



DOI: 10.1021/am508469h
ACS Appl. Mater. Interfaces 2015, 7, 6541−6549

## AUTHOR INFORMATION


### Corresponding Authors

*E-mail: luoyongxiang@mail.sic.ac.cn.
*E-mail: michael.gelinsky@tu-dresden.de. Tel.: +49 351 4586695. Fax: +49 351 4587210.


### Notes

The authors declare no competing financial interest.

## ACKNOWLEDGMENTS

This study was partly funded by the German Federal Ministry for Economics and Technology (BMWi) via AiF. Y.L. would like to thank the Shanghai Municipal Natural Science Foundation (14ZR1445500) and the Natural Science Foundation of China (grant nos. 31400807 and 31370963) for supporting this study. The National High Technology Research and Development Program of China (863 Program, SS2015AA020302) partly supported this study. We thank Dr. Michal Ruhnow (Technische Universität Dresden) for the XRD measurements, Dr. Helene Rahn (Technische Universität Dresden) for performing the $\mu$-CT analysis, and Prof. Dr. Martin Bornhäuser and co-workers (Medical Clinic I, University Hospital Carl Gustav Carus, Dresden) for providing hBMSC.

## REFERENCES


(1) Panagiotis, M. Classification of non-Union. *Injury* **2005**, *36*, 30−37.
(2) Salgado, A. J.; Coutinho, O. P.; Reis, R. L. Bone Tissue Engineering: State of the Art and Future Trends. *Macromol. Biosci.* **2004**, *4*, 743−765.
(3) Yoshimoto, H.; Shin, Y. M.; Terai, H.; Vacanti, J. P. A Biodegradable Nanofiber Scaffold by Electrospinning and its Potential for Bone Tissue Engineering. *Biomaterials* **2003**, *24*, 2077−2082.
(4) Hutmacher, D. W. Scaffolds in Tissue Engineering Bone and Cartilage. *Biomaterials* **2000**, *21*, 2529−2543.
(5) Du, C.; Zhao, J.; Fei, J.; Gao, L.; Cui, W.; Yang, Y.; Li, J. Alginate-Based Microcapsules with a Molecule Recognition Linker and Photosensitizer for the Combined Cancer Treatment. *Chem.—Asian J.* **2013**, *8*, 736−742.
(6) Cui, W.; Cui, Y.; Zhao, J.; Li, J. Fabrication of Tumor Necrosis Factor-Related Apoptosis Inducing Ligand (TRAIL)/ALG Modified $CaCO_3$ as Drug Carriers with the Function of Tumor Selective Recognition. *J. Mater. Chem. B* **2013**, *1*, 1326−1332.
(7) Tønnesen, H. H.; Karlsen, J. Alginate in Drug Delivery Systems. *Drug Dev. Ind. Pharm.* **2002**, *28*, 621−630.
(8) George, M.; Abraham, T. E. Polyionic Hydrocolloids for the Intestinal Delivery of Protein Drugs: Alginate and Chitosan — a Review. *J. Controlled Release* **2006**, *114*, 1−14.
(9) Freeman, I.; Cohen, S. The Influence of the Sequential Delivery of Angiogenic Factors from Affinity-Binding Alginate Scaffolds on Vascularization. *Biomaterials* **2009**, *30*, 2122−2131.
(10) Lee, K. Y.; Mooney, D. J. Alginate: Properties and Biomedical Applications. *Prog. Polym. Sci.* **2012**, *37*, 106−126.
(11) Gombotz, W. R.; Wee, S. F. Protein Release from Alginate Matrices. *Adv. Drug Delivery Rev.* **1998**, *31*, 267−285.
(12) Bajpai, S. K.; Tankhiwale, R. Investigation of Water Uptake Behavior and Stability of Calcium Alginate/Chitosan bi-Polimeric Beads: Part-1. *React. Funct. Polym.* **2006**, *66*, 645−658.
(13) Lin, H. R.; Yeh, Y. J. Porous Alginate/Hydroxyapatite Composite Scaffolds for Bone Tissue Engineering: Preparation, Characterization, and in vitro Studies. *J. Biomed. Mater. Res., Part B* **2004**, *71*, 52−65.
(14) Turco, G.; Marsich, E.; Bellomo, F.; Semeraro, S.; Donati, I.; Brun, F.; Grandolfo, M.; Accardo, A.; Paoletti, S. Alginate/Hydroxyapatite Biocomposite for Bone Ingrowth: A Trabecular Structure with High and Iisotropic Connectivity. *Biomacromolecules* **2009**, *10*, 1575−1583.
(15) Zhang, R.; Ma, P. X. Biomimetic Polymer/Apatite Composite Scaffolds for Mineralized Tissue Engineering. *Macromol. Biosci.* **2004**, *4*, 100−111.
(16) Chen, J.; Chu, B.; Hsiao, B. S. Mineralization of Hydroxyapatite in Electrospun Nanofibrous Poly(L-lactic acid) Scaffolds. *J. Biomed. Mater. Res., Part A* **2006**, *79A*, 307−317.
(17) Murphy, W. L.; Mooney, D. J. Bioinspired Growth of Crystalline Carbonate Apatite on Biodegradable Polymer Substrata. *J. Am. Chem. Soc.* **2002**, *124*, 1910−1917.
(18) Rodriguez, K.; Renneckar, S.; Gatenholm, P. Biomimetic Calcium Phosphate Crystal Mineralization on Electrospun Cellulose-based Scaffolds. *ACS Appl. Mater. Interfaces* **2011**, *3*, 681−689.
(19) Suárez-González, D.; Barnhart, K.; Saito, E.; Vanderby, R.; Hollister, S. J.; Murphy, W. L. Controlled Nucleation of Hydroxyapatite on Alginate Scaffolds for Stem Cell-based Bone Tissue Engineering. *J. Biomed. Mater. Res., Part A* **2010**, *95A*, 222−234.
(20) Yang, D.; Jin, Y.; Zhou, Y.; Ma, G.; Chen, X.; Lu, F.; Nie, J. *In situ* Mineralization of Hydroxyapatite on Electrospun Chitosan-based Nanofibrous Scaffolds. *Macromol. Biosci.* **2008**, *8*, 239−246.
(21) Arafat, M. T.; Lam, C. X. F.; Ekaputra, A. K.; Wong, S. Y.; Li, X.; Gibson, I. Biomimetic Composite Coating on Rapid Prototyped Scaffolds for Bone Tissue Engineering. *Acta Biomater.* **2011**, *7*, 809−820.
(22) Hoyer, B.; Bernhardt, A.; Heinemann, S.; Stachel, I.; Meyer, M.; Gelinsky, M. Biomimetically Mineralized Salmon Collagen Scaffolds for Application in Bone Tissue Engineering. *Biomacromolecules* **2012**, *13*, 1059−1066.
(23) Li, J.; Chen, Y.; Yin, Y.; Yao, F.; Yao, K. Modulation of Nano-Hydroxyapatite Size via Formation on Chitosan−Gelatin Network Film *in situ*. *Biomaterials* **2007**, *28*, 781−790.
(24) Despang, F.; Borner, A.; Dittrich, R.; Tomandl, G.; Pompe, W.; Gelinsky, M. Alginate/Calcium Phosphate Scaffolds with Oriented, Tube-like Pores. *Materialwiss. Werkstofftech.* **2005**, *36*, 761−767.
(25) Xie, M.; Olderøy, M. Ø.; Zhang, Z.; Andreassen, J. P.; Strand, B. L.; Sikorshi, P. Biocomposites Prepared by Alkaline Phosphatase Mediated Mineralization of Alginate Microbeads. *RSC Adv.* **2012**, *2*, 1457−65.
(26) Xie, M.; Olderøy, M. Ø.; Andreassen, J. P.; Selbach, S. M.; Strand, B. L.; Sikorshi, P. Alginate-Controlled Formation of Nanoscale Calcium Carbonate and Hydroxyapatite Mineral Phase within Hydrogel Networks. *Acta Biomater.* **2010**, *6*, 3665−3675.
(27) Zhang, J.; Wang, Q.; Wang, A. *In situ* Generation of Sodium Alginate/Hydroxyapatite Nanocomposite Beads as Drug-Controlled Release Matrices. *Acta Biomater.* **2010**, *6*, 445−454.
(28) Wu, C.; Fan, W.; Gelinsky, M.; Xiao, Y.; Chang, J.; Friis, T.; Cuniberti, G. *In situ* Preparation and Protein Delivery of Silicate−Alginate Composite Microspheres with Core-shell Structure. *J. R. Soc., Interface* **2011**, *8*, 1804−1814.
(29) Chae, T.; Yang, H.; Leung, V.; Ko, F.; Troczynski, T. Novel Biomimetic Hydroxyapatite/Alginate Nanocomposite Fibrous Scaffolds for Bone Tissue Regeneration. *J. Mater. Sci.: Mater. Med.* **2013**, *24*, 1885−1894.
(30) Wu, C.; Luo, Y.; Cuniberti, G.; Xiao, Y.; Gelinsky, M. 3D-Printing of Hierarchical and Tough Mesoporous Bioactive Glass Scaffolds with Controllable Pore Architecture, Excellent Mechanical Strength and Mineralization Ability. *Acta Biomater.* **2011**, *7*, 2644−2650.
(31) Lode, A.; Meißner, K.; Luo, Y.; Sonntag, F.; Glorius, S.; Nies, B.; Vater, C.; Despang, F.; Hanke, T.; Gelinsky, M. Fabrication of Porous Scaffolds by 3D Plotting of a Pasty Calcium Phosphate Bone Cement under Mild Conditions. *J. Tissue Eng. Regener. Med.* **2014**, *8*, 682−693.
(32) Jin, G.; Kim, G. H. Rapid-prototyped PCL/Fucoidan Composite Scaffolds for Bone Tissue Regeneration: Design, Fabrication, and Physical/Biological Properties. *J. Mater. Chem.* **2011**, *21*, 17710−17718.
(33) Luo, Y.; Wu, C.; Lode, A.; Gelinsky, M. Hierarchical Mesoporous Bioactive Glass/Alginate Composite Scaffolds Fabricated



DOI: 10.1021/am508469h
*ACS Appl. Mater. Interfaces* 2015, 7, 6541−6549

by Three-Dimensional Plotting for Bone Tissue Engineering. *Biofabrication* **2013**, *5*, 015005.
(34) Luo, Y.; Lode, A.; Sonntag, F.; Nies, B.; Gelinsky, M. Well-Ordered Biphasic Calcium Phosphate/Alginate Scaffolds Fabricated by Multi-Channel 3D Plotting under Mild Conditions. *J. Mater. Chem. B* **2013**, *1*, 4088−4098.
(35) Khalil, S.; Nam, J.; Sun, W. Multi-nozzle Deposition for Construction of 3D Biopolymer Tissue Scaffolds. *Rapid Prototyping J.* **2005**, *11*, 9−17.
(36) Shkilnyy, A.; Friedrich, A.; Tiersch, B.; Schöne, S.; Fechner, M.; Koetz, J.; Schläpfer, C. W.; Taubert, A. Poly(ethylene imine)-Controlled Calcium Phosphate Mineralization. *Langmuir* **2008**, *24*, 2102−2109.
(37) Shirkhanzadeh, M. Direct Formation of Nanophase Hydroxyapatite on Cathodically Polarized Electrodes. *J. Mater. Sci.: Mater. Med.* **1998**, *9*, 67−72.
(38) Lee, H. J.; Kim, Y. B.; Kim, S. H.; Kim, G. H. Mineralized Biomimetic Collagen/Alginate/Silica Composite Scaffolds Fabricated by a Llow-Temperature Bio-Plotting Process for Hard Tissue Regeneration: Fabrication, Characterisation and *in vitro* Cellular Activities. *J. Mater. Chem. B* **2014**, *2*, 5785−5798.
(39) Zmora, S.; Glicklis, R.; Cohen, S. Tailoring the Pore Architecture in 3-D Alginate Scaffolds by Controlling the Freezing Regime during Fabrication. *Biomaterials* **2002**, *23*, 4087−4094.
(40) Khalil, S.; Sun, W. Bioprinting Endothelial Cells with Alginate for 3D Tissue Constructs. *J. Biomech. Eng.* **2009**, *131*, 111002.
(41) Awad, H. A.; Wickham, M. Q.; Leddy, H. A.; Gimble, J. M. Chondrogenic Differentiation of Adipose-derived Adult Stem Cells in Agarose, Alginate, and Gelatin Scaffolds. *Biomaterials* **2004**, *25*, 3211−3222.
(42) Luo, Y.; Lode, A.; Gelinsky, M. Direct Plotting of Three-Dimensional Hollow Fiber Scaffolds based on Concentrated Alginate Pastes for Tissue Engineering. *Adv. Healthcare Mater.* **2013**, *2*, 777−783.
(43) MacDonald, D. E.; Rapuano, B. E.; Deo, N.; Stranick, M.; Somasundaran, P.; Boskey, A. L. Thermal and Chemical Modification of Titanium−Aluminum−Vanadium Implant Materials: Effects on Surface Properties, Glycoprotein Adsorption, and MG63 Cell Attachment. *Biomaterials* **2004**, *25*, 3135−3146.
(44) Deligianni, D. D.; Katsala, N. D.; Koutsoukos, P. G.; Missirlis, Y. F. Effect of Surface Roughness of Hydroxyapatite on Human Bone Marrow Cell Adhesion, Proliferation, Differentiation and Detachment Strength. *Biomaterials* **2000**, *22*, 87−96.
(45) Kunzler, T. P.; Drobek, T.; Schuler, M.; Spencer, N. D. Systematic Study of Osteoblast and Fibroblast Response to Roughness by means of Surface-Morphology Gradients. *Biomaterials* **2007**, *28*, 2175−2182.
(46) Li, H.; Jia, Y.; Du, M.; Fei, J.; Zhao, J.; Cui, Y.; Li, J. Self-Organization of Honeycomb-like Porous $TiO_2$ Films by means of the Breath-Figure Method for Surface Modification of Titanium Implants. *Chem.—Eur. J.* **2013**, *19*, 5306−5313.
(47) Higuchi, A.; Ling, Q. D.; Hsu, S. T.; Umezawa, A. Biomimetic Cell Culture Protein as Extracellular Matrices for Stem Cell Differentiation. *Chem. Rev.* **2012**, *112*, 4507−4540.
(48) Chung, T. W.; Yang, J.; Akaike, T.; Cho, K. Y.; Nah, J. W.; Kim, S. I.; Cho, C. S. Preparation of Alginate/Galactosylated Chitosan Scaffold for Hepatocyte Attachment. *Biomaterials* **2002**, *23*, 2827−2834.
(49) Shachar, M.; Tsur-Gang, O.; Dvir, T.; Leor, J.; Cohen, S. The Effect of Immobilized RGD Peptide in Alginate Scaffolds on Cardiac Tissue Engineering. *Acta Biomater.* **2011**, *7*, 152−162.
(50) Kilian, K. A.; Bugarija, B.; Lahn, B. T.; Mrksich, M. Geometric Cues for Directing the Differentiation of Mesenchymal Stem Cells. *Proc. Natl. Acad. Sci. U.S.A.* **2010**, *107*, 4872−4877.
(51) Treiser, M. D.; Yang, E. H.; Gordonov, S.; Cohen, D. M.; Androulakis, I. P.; Kohn, J.; Chen, C. S.; Moghe, P. V. Cytoskeleton-based Forecasting of Stem Cell Lineage Fates. *Proc. Natl. Acad. Sci. U.S.A.* **2010**, *107*, 610−615.
(52) Kumar, G.; Waters, M. S.; Farooque, T. M.; Young, M. F.; Simon, C. G., Jr. Freeform Fabricated Scaffolds with Roughened Struts that Enhance both Stem Cell Proliferation and Differentiation by Controlling Cell Shape. *Biomaterials* **2012**, *33*, 4022−4030.


DOI: 10.1021/am508469h
*ACS Appl. Mater. Interfaces* 2015, 7, 6541−6549